 doi:10.20944/preprints202209.0251.v1

Article

Applicability of Asymmetric Specimens for Residual Stress Evaluation in Fiber Metal Laminates

Johannes Wiedemann [1,†,*], Jan-Uwe R. Schmidt [1,†] and Christian Hühne [1,2]

[1] TU Braunschweig, Institute of Mechanics and Adaptronics, Langer Kamp 6, 38106 Braunschweig, Germany
[2] DLR, Institute of Composite Structures and Adaptive Systems, Lilienthalplatz 7, 38108 Braunschweig, Germany
* Correspondence: johannes.wiedemann@tu-braunschweig.de
† These authors contributed equally to this work

Abstract: Residual stresses in fiber metal laminates (FML) inevitably develop during the manufacturing process. The main contributor to these stresses is the difference in the coefficients of thermal expansion (CTE) between fibers and metal in combination with high process temperatures. To quantify these stresses, the use of specimens with an asymmetric layup is an easily adaptable method. The curvature that develops after the manufacturing of flat laminates with an asymmetrical layer stack is a measure of the level of residual stresses evolving during cure. However, the accuracy of the curvature evaluation is highly dependent on specimen design and other influencing parameters. In this work a large set of FML specimens is investigated to identify relevant influencing parameters and derive conclusions about specimen design and evaluation techniques. For certain layups and process parameters, there is a good correlation between the curvature and the stress-free temperature, which is further covered by analytical solutions for bimetals. This correlation is the basis to transfer curvature into a stress-free temperature that can consequently be used for the quantification of residual stress levels in more complex FMLs. The transfer is validated by in-situ strain measurements during cure using a strain gage technique. Based on the results, the application of asymmetric specimens for residual stress characterization in more complex laminates is presented in the form of a workflow.

Keywords: fiber metal laminate; hybrid laminate; residual stress; asymmetric laminate; process monitoring; curvature analysis; stress-free temperature

1. Introduction

Fiber metal laminates (FML) are an advanced intrinsic hybrid material made from composites and metals [1]. FMLs are specifically designed for applications that would not be feasible with monolithic materials alone. The most prominent FML material arose from the goal of improving conventional aluminum for aerospace applications by laminating layers of glass fiber reinforced polymer together with thin sheets of aluminum. The result is a glass fiber reinforced aluminum (GLARE) that possesses superior damage tolerance and fatigue behavior compared to structures made from monolithic aluminum [2]. Contrastingly, applications evolved where the properties of monolithic composite materials are improved by reinforcing the material with thin metal sheets (mainly titanium and steel), for example, for load introduction zones [3], crash elements [4] or erosion protection [5].

However, residual stresses arise in the manufacturing process due to the different coefficients of thermal expansion (CTE) and the high stiffness of fibers and metal combined with high temperatures during manufacturing. These stresses can lead to early component failure and act as damage initiators during fatigue loading [6]. The residual stresses can account for around 20 % of the material strength dependent on the material combination, layup, and operating temperature [7,8]. Hence, it is obvious that residual stresses should be considered during the design process of FML structures.

Preprints (www.preprints.org) | NOT PEER-REVIEWED | Posted: 19 September 2022 doi:10.20944/preprints202209.0251.v1

Table 1. Asymmetric specimens made of carbon fiber reinforced polymer (CFRP) or fiber metal laminates (FML) used in the literature vary greatly in their dimensions and laminate layups

Material	Source	Dimensions [mm^2]	Width-to-length ratio	Layup	Thickness [mm]
CFRP	[19]	25 x 152	0.16	$0_3/90_3$	0.75
CFRP	[15]	100 x 230[a]	0.4	0/90	0.25
CFRP	[14]	25/11 x 152	0.16/0.07	$0_4/90_4$	-
CFRP	[16]	25 x 150	0.16	$90_4/0_2$, $90_2/0_2$, $90_2/0$	0.4-0.8
FML	[17]	20 x 200	0.1	$St/0$	0.25
FML	[12]	100 x 200	0.5	$St/0_3$	0.5
FML	This work	20 x 290[a]	0.07	cf. Table 7	0.5 - 1.0

[a] trimmed

For this purpose, the residual stress level in a manufactured component must be reliably quantified, for which a variety of methods exists in the literature. Based on [9], these can be divided into destructive and non-destructive methods, as well as methods that monitor the strains during the manufacturing process and those which try to make conclusions about the internal stress state of a specimen after manufacturing. The most accurate methods certainly are integrated or applied sensors that are capable of measuring the strains in-situ during the manufacturing process. Recently, mainly fiber optic sensors (FOS), especially fiber Bragg grating (FBG) sensors (e.g. [10–12]), as well as strain gages (e.g. [7,13]) were used in the literature.

The disadvantage of these sensors is the complex experimental setup which is not suitable for continuous monitoring during industrial manufacturing processes. The curvature measurement, instead, seems to be a great option for industrial applications since the complexity during manufacturing is low, and the evaluation process can be transferred to the time after manufacturing. This method is also very prominent in the literature, e.g. [14–16] to determine the residual stresses developing in thermoplastic and thermoset carbon fiber reinforced composites. Beyond these investigations, [17] already used the curvature analysis for asymmetric FML specimens. In [9], however, it is stated that warpage or curvature measurements go along with limited accuracy of the results. Likewise, in [17] different evaluated parameters of curved laminates (curvature and stress-free temperature) show large deviations among themselves. It is assumed that the layup, laminate thickness, and dimensions of the specimens play a great role in terms of evaluation reliability besides the manufacturing process itself.

To get an overview of specimen dimensions and layups that were used in the literature, Table 1 lists some sources with their corresponding asymmetric specimen architectures made of monolithic carbon fiber reinforced polymer (CFRP) or FML. The size of the specimens and the layups vary greatly among them. For small aspect ratios (width-to-length), the curvature in the transverse direction only influences the main curvature to a minor degree. With aspect ratios close to 1, a saddle-shape curvature or a bi-stable deflection behavior is expected [16,18]. Therefore a width-to-length ratio of 0.07 is chosen in this work, whereas different layups and consequent laminate thicknesses are evaluated.

Asymmetric laminates cannot only be investigated in terms of curvature but also their stress-free temperature T_{sf} can be analyzed, e.g. [20–22]. The T_{sf} is determined as that temperature at which curved laminates transition back into their initial plane state. Most of the time, the T_{sf} is somewhere below the final cure temperature of the laminate [23,24]. The T_{sf} is the relevant parameter when manufacturing-induced thermo-mechanical stresses need to be calculated in a laminate. Therefore, stress-free temperatures will likewise be evaluated in this work and correlated to measured curvatures using analytical and numerical methods.

 doi:10.20944/preprints202209.0251.v1

Table 2. Parameters influencing the residual stress state and variations investigated in this work

Parameter	Variation
Layup	No. of CFRP and steel plies (varying laminate thicknesses and metal volume fractions)
Manufacturing setup	single specimen on tool and two specimens stacked on top of each other
Tool material	steel (S) and aluminum (A)
Cure cycle	manufacturer recommended (MRCC) and modified cure cycle (MOD)

Both parameters, curvature and stress-free temperature, are sensitive to several influencing factors, that contribute to the residual stress state. These factors can generally be divided into intrinsic and extrinsic parameters [25,26]. Intrinsic parameters include material and layup-dependent anisotropy, whereas extrinsic parameters include tool and process influences. Although the different parameters are mainly investigated for monolithic FRP materials, the results can be equally transferred to FMLs. For FMLs however, the intrinsic anisotropy due to large differences in the coefficients of thermal expansion of the single constituents, plays a greater role than for monolithic FRP.

The tool is a main extrinsic parameter affecting the residual stress state which mainly results from incompatibility in thermal expansion between tool and laminate. Two phenomena are differentiated in the literature, which are forced interaction [26,27] and warpage [26, 28]. Since the laminates are manufactured in a plane state, no geometrical interlocking between the tool and composite part is present. Therefore, only the effect of warpage needs to be considered. Warpage mainly occurs for thin laminate thicknesses ($t \leq 1\,\mathrm{mm}$) in combination with large CTE differences between tool material and laminate [25]. Table 1 shows that the specimen architectures of the asymmetric specimens used in the literature are within the relevant thickness range for warpage and hence this effect needs to be considered during the evaluation.

The other extrinsic parameter of interest is the cure cycle itself. It was shown, that residual stress levels in a composite laminate can be directly influenced by modifying the temperature profile during cure [29–32]. The idea behind these modified cure cycles for thermoset resins is the shift of the gel point of the resin to a temperature as close as possible to room or operating temperature. By integrating intermediate cooling steps into the cure cycle, this can be achieved and consequently thermal residual stresses can be reduced.

The range of influences shows that a comprehensive understanding of the effect of the different parameters on the residual stress state and hence on the curvature of an asymmetric specimen is necessary, to develop a reliable method that uses curvature analysis for process monitoring and for residual stress quantification.

The general objective of this work is to describe a method that uses information from simple asymmetric laminates to determine the residual stress state in a more complex FML structure. The methodology should be easy to apply and provide good repeatable results. For this purpose, the influence of various relevant parameters on the curvature of asymmetric specimens is investigated and recommendations for specimen design are given.

Section 2 explains all the relevant methods used in this work and introduces the materials and specimen manufacturing process. Subsequently, intrinsic and extrinsic parameters and their influence on the deformation behavior of asymmetric laminates are investigated. Table 2 gives an overview of the different parameter variations investigated in this work. In preliminary considerations, the influence and suitability of different specimen layups are discussed (Section 3.1.1). Furthermore, recommendations for manufacturing are derived from different manufacturing setups. Consequently, the two main extrinsic factors, tool material (Section 3.1.2) and cure cycle modifications (Section 3.1.3) are discussed in terms of their influence on the curvature.

Different methods are compared to evaluate the curvature and stress-free temperature of asymmetric specimens. Based on this, recommendations are given to ensure a robust

 doi:10.20944/preprints202209.0251.v1

evaluation process. Using analytics and finite element analysis (FEA), the experimentally determined quantities are related to each other (Section 3.2). The measured quantities are transformed into a predominant stress state using the classical laminate theory. To validate this transformation, a strain-gage method to measure the cure strains during manufacturing is used [8] (Section 3.3).

Finally, based on the knowledge gained, a workflow is proposed (Figure 16 in Section 4) which summarizes the necessary steps from manufacturing to evaluation of the asymmetric laminates and consequent calculation of the residual stress state for a more complex FML structure.

2. Materials and Methods

This section explains the methods to evaluate different parameters of asymmetric laminates (Section 2.1). Analytical and numerical relations between curvature and stress-free temperature are given (Section 2.2 and 2.3), besides the relevant formulas to transfer stress-free temperature into corresponding residual stresses (Section 2.4). Subsequently, a description of the manufacturing processes (Section 2.5) and a definition of used materials and specimen architectures is presented (Section 2.6).

2.1. Methods for the evaluation of asymmetric specimen

All the different methods to evaluate manufactured asymmetric specimens are described in this section. The evaluation parameters of interest are the curvature, the stress-free temperature, as well as the cure strains developing during manufacturing. The cure strain measurements are used for validation purposes later in this work.

2.1.1. Curvature measurements

Two different techniques are used for the curvature analysis in this work. The curvature is measured during the preliminary investigations with a laser distance sensor attached to a 2-dimensional gantry. This technique allows to evaluate the distance between curved specimen and sensor for discrete points (see Figure 1a). A 2-dimensional contour plot is generated this way and by calculating a fitting curve, the radius of the specimen is determined. However, this approach showed to be very time-consuming and includes difficulties for large curvatures due to the measurement range of the laser sensor and reflection issues. Therefore, an industrial 3-dimensional scanning head (GOM ATOS) is used for the subsequent experiments. The GOM ATOS scan generates a point cloud of the specimen, which is consequently analyzed using the GOM-Inspect software. By fitting a cylinder into the point cloud, the radius of the specimens is determined (see Figure 1b). An additional advantage of using the GOM ATOS scan is the possibility to evaluate not only the specimen curvature but also the laminate thickness, as well as the thickness distribution.

2.1.2. Stress-free temperature measurement

The stress-free temperature of all specimens is determined in a lab oven with a glass window. The setup for a single specimen is shown in Figure 2. The specimens are placed on a metal plate in the oven (see Figure 2a) and are subsequently heated from room temperature to 140 °C with a heating ramp of $4\,\mathrm{K\,min^{-1}}$. At this temperature, they are allowed to equalize for 30 min before being heated slowly with a heating rate of $0.7\,\mathrm{K\,min^{-1}}$ up to the stress-free temperature. The stress-free state is visually determined when all specimen edges are in contact with the bottom plate (see Figure 2b). The temperature is measured with several type K thermocouples located on the bottom plate to assure a homogeneous temperature distribution. The determination of the stress-free temperature is a visual technique and highly depends on the person conducting the experiment. Therefore, the repeatability and accuracy of the measurement is estimated by repeating a measurement for identical specimens. It can be assumed that the accuracy of this technique is within a range of ± 3 °C.

Preprints (www.preprints.org) | NOT PEER-REVIEWED | Posted: 19 September 2022 doi:10.20944/preprints202209.0251.v1

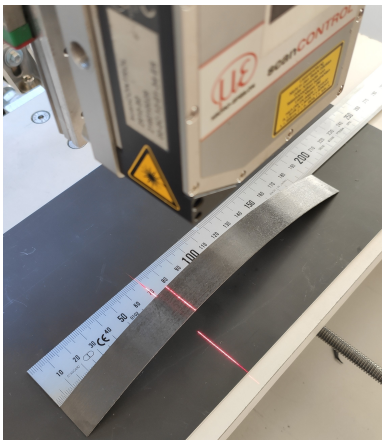

(a) Laser distance sensor for specimen height evaluation

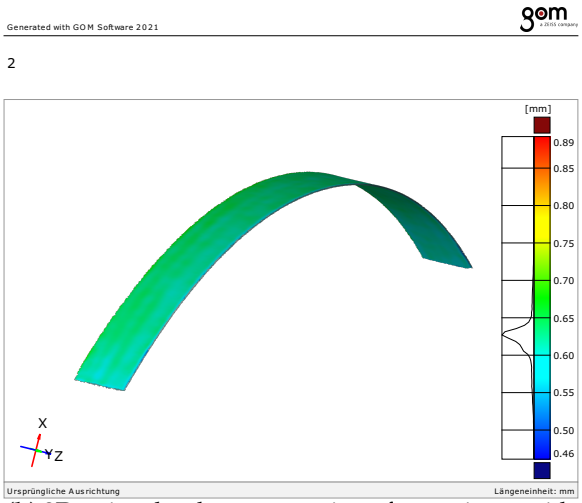

(b) 3D point cloud representation of a specimen with GOM ATOS (legend indicates the laminate thickness)

Figure 1. Measurement techniques for the curvature evaluation of asymmetric specimens

(a) Curved specimen at room temperature

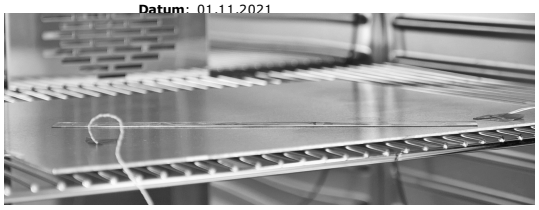

(b) Flat specimen at stress-free temperature 2/2

Figure 2. Stress-free temperature measurement through reheating of a specimen after manufacturing in a lab oven and determination of the temperature when the specimen reaches its flat state

2.1.3. Strain gage technique

The curvature analysis and stress-free temperature measurements are validated by the means of an instrumented specimen equipped with a strain gage (SG) using a technique previously described in [7,8]. A strain gage is bonded to the top metal ply in the fiber direction prior to manufacturing and the strains during the entire manufacturing process are recorded such that the residual strains at the end of the cure cycle are determined directly. Hence, measured residual strains can be correlated to stress-free temperatures and measured curvatures of the same specimen using the classical laminate theory (CLT). The experimental setup is illustrated in Figure 3. The specimen is placed with the CFRP layers onto the tool surface. The strain gage bonded to the top metal ply is contacted through a cut-out in the cover plate. A dummy strain gage bonded to an ultra-low expansion (ULE) glass specimen is placed next to the asymmetric specimen in the autoclave to compensate for any temperature-induced strains in the strain gage itself. The temperatures are monitored with thermocouples placed inside the laminate and on the ULE glass specimen. For more details about this technique, the reader is referred to [7,8].

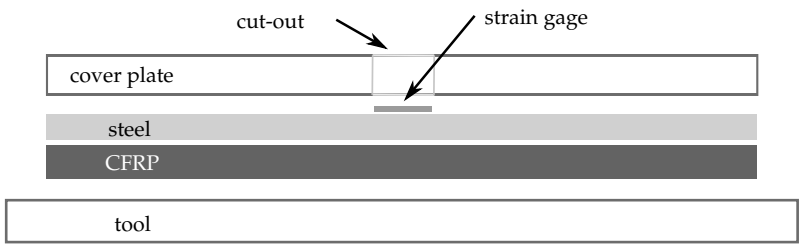

Figure 3. Manufacturing setup for specimen equipped with strain gage

Preprints (www.preprints.org) | NOT PEER-REVIEWED | Posted: 19 September 2022 doi:10.20944/preprints202209.0251.v1

2.2. Analytical correlation between curvature and stress-free temperature

Several analytical models to describe the curvature of asymmetric laminates after manufacturing are found in the literature [33–35]. The analytical approaches mainly originate from bimetal applications where two different metallic layers are joined together to produce a thermomechanical bending transducer. The most comprehensive analytical description to calculate the radius r of such bi-materials dependent on a reference temperature is given by Timoshenko [35]:

$$r = \frac{h(3(1+m)^2 + (1+m\cdot n)(m^2 + \frac{1}{m\cdot n}))}{6\cdot(\alpha_2 - \alpha_1)(T_{sf} - T_r)(1+m)^2} \tag{1}$$

where h is the specimen thickness, α_1 and α_2 are the coefficients of thermal expansion for the two materials, T_r is the reference temperature, and T_{sf} is the stress-free temperature. $m = {}^{t_1}/_{t_2}$ represents the ratio of the thicknesses (t_1 and t_2) of the two constituents (FRP and steel), whereas $n = {}^{E_1}/_{E_2}$ indicates the ratio of the elastic moduli of the two constituents (FRP and steel), respectively.

This equation is widely used in the literature for the description of curvatures of asymmetric CFRP laminates [16,33] and FML [22] and will therefore also be used in this work to correlate the radius and stress-free temperature of different asymmetric laminates with each other. The applicability of the analytical description in the context of this work will be discussed in the results section.

2.3. Numerical correlation between curvature and stress-free temperature

Besides the analytical curvature calculation, also finite element analysis is used for the validation. In the FEA, the experiment to determine the stress-free temperature based on a given curvature as described in section 2.1 is modeled using the FEA software Abaqus.

A curved specimen is created using a shell section and given the radius derived from the GOM ATOS measurements. The laminate layup and the respective material properties are assigned to the shell section and the part is meshed using quadrilateral shell elements with reduced integration (type S8R). Subsequently, the specimen is placed on a flat surface consisting of rigid body elements. Because of the large deformations, a non-linear calculation is pursued. A temperature step is included in the model to achieve the deformation by heating the specimen from room temperature to a higher temperature level. Using a Python script, the temperature at which the curved specimen transitions into its flat state is determined iteratively. The flat state is defined when the nodes at the short specimen edges have identical Y-coordinates compared to the center nodes as shown in Figure 4. Consequently, the resulting temperature is defined as the stress-free temperature of the investigated specimen.

In the results section, the numerical outcomes are compared to the experiments and analytical calculations.

2.4. Transformation of stress-free temperature into residual stresses

With the stress-free temperature known, the residual stresses in an arbitrary laminate can be calculated with the classical laminate theory. When assuming purely linear thermoelastic behavior, the ply-wise residual stresses for unidirectional symmetric layups, are given by the following equation [8]:

$$\{\sigma_{res}\}_k = [Q]_k \cdot \Big((\{\alpha\}_{lam} - \{\alpha\}_k) \cdot \Big(T_R - T_{sf} \Big) \Big) \tag{2}$$

with the reduced stiffness matrix $[Q]_k$ for each ply k, the coefficients of thermal expansion $\{\alpha\}_k$ per ply and for the entire laminate $\{\alpha\}_{lam}$. The parameter T_R specifies the reference temperature, e.g. operating temperature or room temperature, whereas T_{sf} indicates the stress-free temperature derived from experiment or calculation.

Preprints (www.preprints.org) | NOT PEER-REVIEWED | Posted: 19 September 2022 doi:10.20944/preprints202209.0251.v1

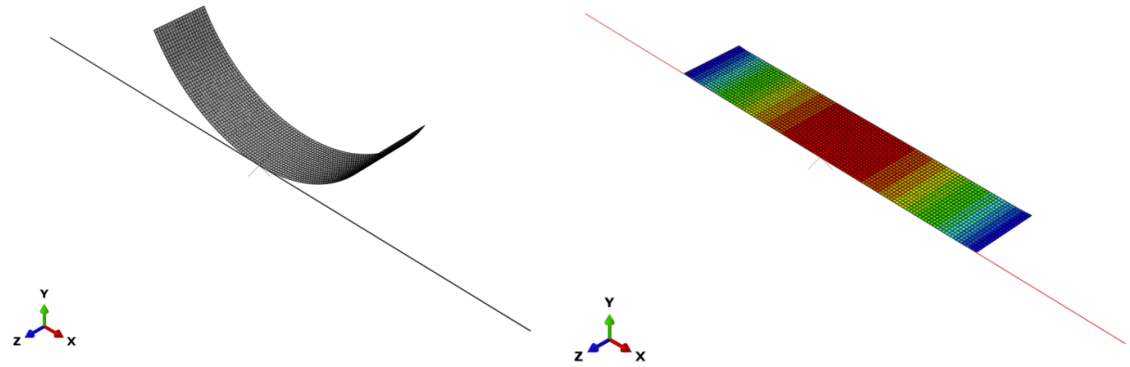

(a) Curved specimen in its initial state **(b)** Flat specimen after applied temperature change

Figure 4. FEA model to determine the stress-free temperature for a given curvature of an asymmetric specimen

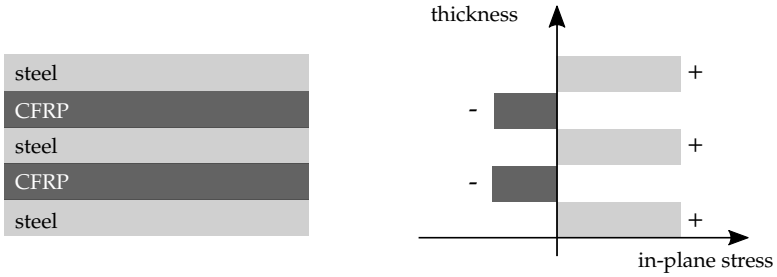

Figure 5. Residual stress state through the thickness in a generic FML after manufacturing at elevated temperature and cool down to room temperature

The in-plane laminate thermal expansion coefficient $\{\alpha\}_{lam}$ can be derived from the ply CTEs with Equation 3 for an arbitrary laminate [8]:

$$\{\alpha\}_{lam} = [R]^{-1} \cdot [A]^{-1} \cdot \sum_{k=1}^{n} [\overline{Q}]_k \cdot [R] \cdot [T]_k^{-1} \cdot t_k \cdot \{\alpha\}_k \tag{3}$$

$$\text{with } [R] = \begin{bmatrix} 1 & 0 & 0 \\ 0 & 1 & 0 \\ 0 & 0 & 2 \end{bmatrix} \quad \text{and } [T] = \begin{bmatrix} c^2 & s^2 & 2sc \\ s^2 & c^2 & -2sc \\ -sc & sc & c^2 - s^2 \end{bmatrix}$$

where $[A]$ is the laminate extensional stiffness matrix, $[\overline{Q}]_k$ the ply stiffness in global laminate coordinates, $[T]$ the transformation matrix and t_k the thickness for each ply respectively. Again, $\{\alpha\}_k$ indicates the coefficients of thermal expansion for the respective ply. In the transformation matrix, s and c indicate the $sin(\alpha)$ and $cos(\alpha)$ terms, where α is the ply angle in the laminate coordinate system. Further information can be found for example in [23,36].

Figure 5 exemplarily shows the stress state of an arbitrary laminate consisting of three steel and two CFRP plies. The coefficient of thermal expansion of the metal plies is generally multiple times higher than the CTE of the fiber plies in the fiber direction. Hence, after curing at elevated temperature, and cooling down to room temperature, tensile residual stresses dominate in the metal plies and compressive residual stresses prevail in the fiber plies in the fiber direction. Therefore, the asymmetric laminates considered in this work are always bending towards the steel layer after manufacturing, as part of the residual stresses can be relieved this way.

Preprints (www.preprints.org) | NOT PEER-REVIEWED | Posted: 19 September 2022 doi:10.20944/preprints202209.0251.v1

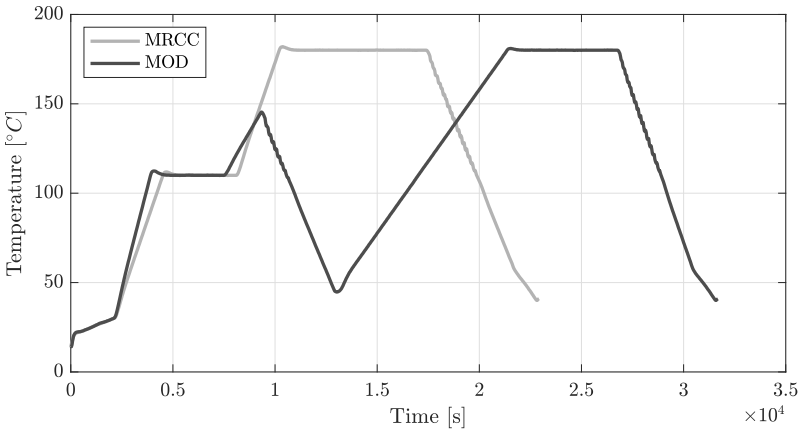

Figure 6. Two different temperature profiles during autoclave cure for the two considered manufacturing processes MRCC and MOD

2.5. Manufacturing of asymmetric laminates

This section illustrates the two steps during manufacturing of the asymmetric laminates. The first step is the manufacturing process itself, the second step includes the post-processing of the asymmetric laminates.

2.5.1. Manufacturing process

The manufacturing process used for the FMLs in this work is very similar to the manufacturing process for FRP parts using prepreg materials which is a standard in the aerospace industry. The only difference is the metal sheets that need appropriate preprocessing to assure good adhesion with the resin material and consequently a good interlaminar shear strength. For this purpose, different techniques have been investigated in the literature [37]. The mechanical cleaning using a vacuum suction blasting process in combination with an aqueous sol-gel solution has proven to produce mechanically compliant laminates without being environmentally harmful [38,39]. This manufacturing strategy is consequently used in this work. After mechanical cleaning, the steel sheets are chemically cleaned with heptane before a layer of 3M Surface Pre-Treatment AC-130-2 [40] is applied. The steel sheets are laminated immediately after the required drying period.

The FMLs are manufactured between a metal tool and a cover plate under a vacuum bag in an autoclave. To investigate the influence of the curing process itself, laminates with two different cure cycles are manufactured. One is the manufacturer-recommended cure cycle (MRCC), and the other is a modified cure cycle (MOD) that has been proven to significantly lower the residual stress state in an FML [8,22]. The two cure cycles are depicted in Figure 6. The MRCC is a two-hold cure cycle with a consolidation stage at 110 °C and a final cure stage at 180 °C, whereas the MOD cure cycle includes an intermediate cooling step to move the gel point of the resin to a lower temperature level. This way, the temperature of final bonding is lower and so are the final residual stresses in the laminate at room temperature.

Three different strategies on how to place the asymmetric laminates between the tool and cover plate are compared in this work. These three different setups are depicted in Figure 7. For the first two options, the laminate is placed between the tool and cover plate either with the CFRP side or the steel side onto the tool surface. The third option is a setup that includes the manufacturing of two specimens at once while they are placed on top of each other with a Teflon release film in between to allow separation after manufacturing. This setup was used by [17] in the literature. The advantage of the second setup is less space requirement on the tool surface and the need for only one cover plate per two specimens. Although the tool material is varied during the experiments in this work, the material of the cover plate and tool is always identical for all investigated configurations.

Preprints (www.preprints.org) | NOT PEER-REVIEWED | Posted: 19 September 2022 doi:10.20944/preprints202209.0251.v1

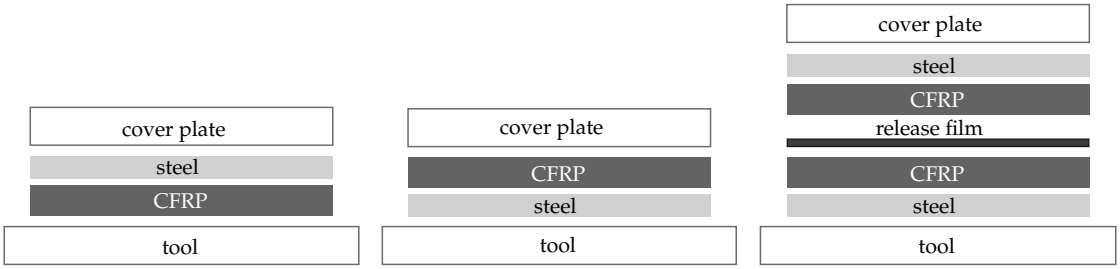

(a) Single setup: CFRP on tool **(b)** Single setup: steel on tool **(c)** Stacked setup

Figure 7. Different manufacturing setups regarding the placement of the layer stack between tool and cover plate

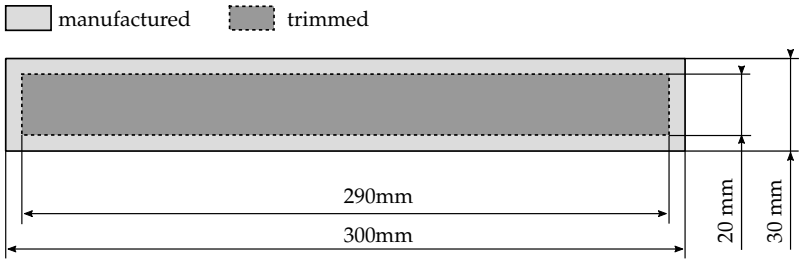

Figure 8. Dimensions of the manufactured and trimmed specimens in their plane state

2.5.2. Postprocessing

The specimens are manufactured with a size of 300 mm by 30 mm, resulting in an aspect ratio of 10:1. This way, the specimen curvature will be dominant in one direction and influences of the transverse curvature can be minimized. After manufacturing, the edges of the specimens are trimmed to reduce the influence of edge effects. These edge effects originate from a slight decrease in thickness towards the specimen edges due to resin bleed. From Figure 1b it can be seen that the thickness of the trimmed specimen is very much evenly distributed over the entire specimen. The dimensions of the manufactured and trimmed specimens are illustrated in Figure 8. It needs to be emphasized, that manufacturing and trimming are always performed in the specimens' flat state by applying external loads onto the specimens. The curvature of the specimens is restored when they are free of any external forces.

It is assumed that the cutting process can potentially influence the curvature of the specimen. During the manufacturing of the first specimens, a circular saw with a diamond blade was used for cutting. This process led to uneven edges and local edge delaminations in the specimens. Furthermore, local heat generation which can potentially change the specimen state can not be excluded. Therefore, for the subsequent investigations water jet cutting was used for the trimming of the specimens. With this process no heat is generated in the specimens, the roughness of the edges is reduced significantly, and no edge delaminations are observed.

2.6. Definition of materials and specimen

The FML laminates in this work are manufactured from a high-strength stainless steel alloy 1.4310 (X10CrNi18-8) and carbon fiber reinforced epoxy prepreg Hexply 8552-AS4 from the Hexcel company. Because of possible anisotropy due to the rolling process of the thin metal sheets, as reported in the literature [3], the elastic modulus for the steel alloy was tested in a tensile test machine for the two principal in-plane directions. The tensile tests were performed according to DIN EN ISO 6892-1 [41] with rectangular specimen (260 mm x 20 mm). The results of the tensile tests are shown in Figure 9.

A consistent behavior can be seen over all the single specimens. Consequently, this results in a small relative standard deviation (RSD) of 0.65 % in the rolling direction and 2.73 % transverse to the direction of rolling as can be found in Table 3. The difference in the

Preprints (www.preprints.org) | NOT PEER-REVIEWED | Posted: 19 September 2022 doi:10.20944/preprints202209.0251.v1

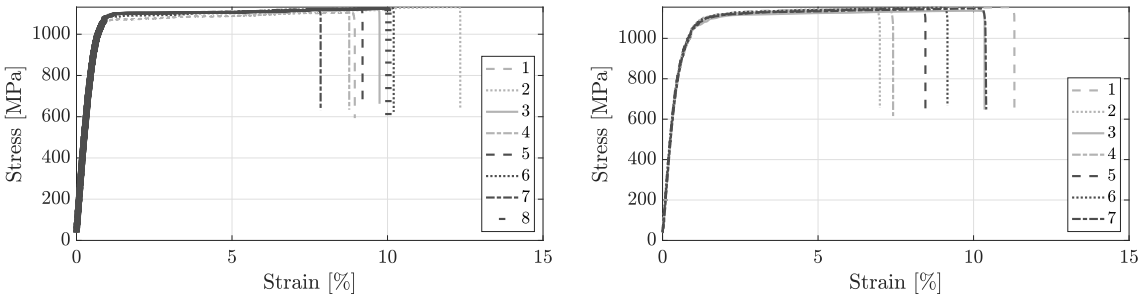

(a) Stress strain curve in direction of rolling (DOR) **(b)** Stress strain curve transverse to DOR

Figure 9. Stress over strain resulting from tensile tests to determine the Young's modulus of cold rolled 1.4310 stainless steel

Table 3. Results of tensile tests on the 1.4310 steel are given as the mean value and the relative standard deviation. The direction of rolling of the steel material is indicated by the index 1, while the index 2 denotes the transverse direction.

	E_1	$\sigma_{1,ult}$	E_2	$\sigma_{2,ult}$
Mean	187 GPa	1121 MPa	194 GPa	1147 MPa
RSD	1.15 %	0.65 %	2.73 %	0.48 %

elastic modulus for the two principal in-plane directions of around 7 GPa is in accordance with the literature, e.g. [3].

All other material properties for the CFRP and steel that are used during the subsequent evaluations are taken from the literature and provided in Table 4.

3. Results

The results in this work are based on a specimen program consisting of 47 asymmetric laminates. The specimens mainly differ in their layup and manufacturing strategy, as well as in the tool material and process cycle used. Table 5 gives an overview of all the specimens and their respective parameters. Every single specimen is given an ID during the manufacturing process. In this work, however, specimens with identical influencing parameters, are condensed into a single ID, whereas during the evaluation the mean value together with the respective standard deviation is always shown.

The identifier of the sample is developed so that the parameter variation in the parameter space is evident from the identifier itself. An explanation of the specimen labeling is given in Table 6 using the specimen with ID14SR-s as an example. The first two digits

Table 4. Material properties for the single constituents of the CFRP-steel laminates used in this work. The fiber direction (CFRP) and direction of rolling (steel) is indicated by the index 1, while the index 2 denotes the transverse direction. The superscripts t and c distinguish the properties in tension and compression

Value	Unit	Hexcel 8552-AS4	Steel 1.4310
E_1^t	GPa	132 [42]	187 (this work)
E_1^c	GPa	116 [42]	-
E_2^t	GPa	9.2 [42]	194 (this work)
E_2^c	GPa	9.9 [42]	-
G_{12}	GPa	4.8 [42]	71.2 [12]
ν_{12}	-	0.3 [42]	0.3 [12]
t_{ply}	mm	0.13[b] [43]	0.12
α_1	ppm/K	0.4 [44]	19.0 [8]
α_2	ppm/K	31.2 [44]	19.15 [8]

[b] cured

Preprints (www.preprints.org) | NOT PEER-REVIEWED | Posted: 19 September 2022 doi:10.20944/preprints202209.0251.v1

Table 5. Overview of the specimen program and its parameter variations in this work

ID	Layup	Tool	Cure cycle	Setup	CFRP batch	Quantity
13AR-e	$St/0_3$	A	MRCC	single	expired	3
14SR	$St/0_4$	S	MRCC	single	new	4
14SR-s	$St/0_4$	S	MRCC	stack	new	4
14SM	$St/0_4$	S	MOD	single	new	2
14AR	$St/0_4$	A	MRCC	single	new	1
14AR-e	$St/0_4$	A	MRCC	single	expired	3
14AR-s	$St/0_4$	A	MRCC	stack	new	2
14AM	$St/0_4$	A	MOD	single	new	2
15AR	$St/0_5$	A	MRCC	single	new	3
17SR	$St/0_7$	S	MRCC	single	new	4
17SR-s	$St/0_7$	S	MRCC	stack	new	4
17SM	$St/0_7$	S	MOD	single	new	3
17AR	$St/0_7$	A	MRCC	single	new	1
17AR-e	$St/0_7$	A	MRCC	single	expired	3
17AR-s	$St/0_7$	A	MRCC	stack	new	3
17AM	$St/0_7$	A	MOD	single	new	3
1412AR	$St/0_4/St/0_2$	A	MRCC	single	new	2
					SUM	47

Table 6. Explanation of the logic that is used to label every specimen manufactured, using the specimen with ID14SR-s as an example

1	No. of steel plies	-
4	No. of CFRP plies	-
S	Tool material	S: steel / A: aluminum
R	Cure cycle	R: recommended / M: modified
-s	Additional information	-s: stacked manufacturing setup / -e: expired CFRP batch

indicate the number of steel and CFRP plies within the laminate. The next two digits specify the tool material, the specimen was manufactured on and the cure cycle (cf. Figure 6). The last digit indicates the manufacturing setup as discussed in Figure 7, as well as the CFRP batch used.

During the preliminary investigations, an expired batch of CFRP material was used besides a new material batch. Due to a high number of freeze-thaw cycles, the initial degree of cure of the expired material is different from the new material and consequently, comparisons across both material batches will lead to erroneous conclusions. Therefore, the specimens manufactured with the expired CFRP batch will only be taken into account during the preliminary considerations regarding layup, where the deviation between the different layups is greater than the effect of the CFRP batch and hence, the conclusions drawn are valid. Thereafter, specimens made from the expired CFRP batch will be excluded from the discussion.

Every single specimen is evaluated for its respective curvature and stress-free temperature. As discussed in Section 2.2, there is a correlation between curvature and stress-free temperature. However, since the curvature measurement is easier and more accurate compared to the visual T_{sf}-determination, the influence of the different parameters is discussed in Section 3.1 using the curvature only. Nevertheless, the same conclusions can be drawn using the stress-free temperature, which is shown in Section 3.2, where the two parameters are correlated with each other.

Preprints (www.preprints.org) | NOT PEER-REVIEWED | Posted: 19 September 2022 doi:10.20944/preprints202209.0251.v1

Table 7. Layup variations investigated in this work and resulting metal volume fractions (MVF) and nominal laminate thicknesses. Layups in bold print are chosen for the subsequent investigations

ID	Layup	Metal volume fraction (MVF) [%]	Nominal thickness [mm]
13...	$St/0_3$	24	0.51
14...	$\boldsymbol{St/0_4}$	**19**	**0.64**
15...	$St/0_5$	16	0.77
17...	$\boldsymbol{St/0_7}$	**12**	**1.03**
1412...	$St/0_4/St/0_2$	24	1.02

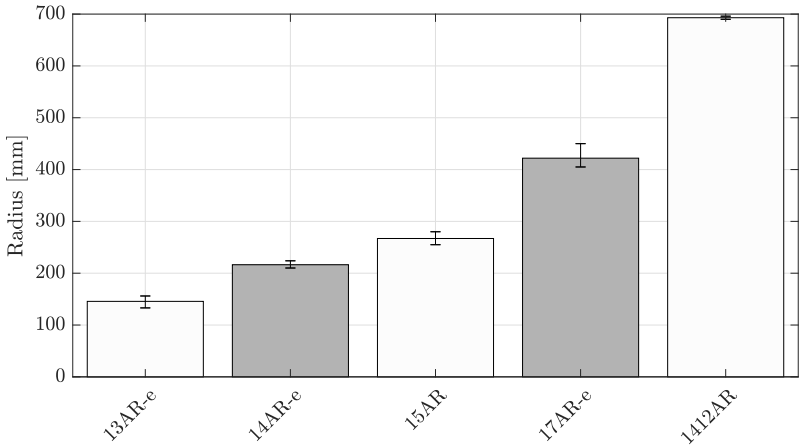

Figure 10. Variations in the layup and consequent specimen thicknesses result in significantly different radii of the asymmetric specimen

3.1. Experimental curvature analysis

To keep manufacturing efforts within limits, certain FML layups are selected for subsequent investigations during a preliminary study (Section 3.1.1). Subsequently, the influence of tool material (Section 3.1.2) and process modification (Section 3.1.3) on the specimen curvature is evaluated for the selected layups. In the end, all relevant curvatures are compared and conclusions regarding the influence of the manufacturing setup are drawn (Section 3.1.4).

3.1.1. Preliminary considerations regarding layup

In the literature, many different layup configurations for asymmetric laminates are selected (cf. Table 1). However, the question arises which type of laminate layup is most appropriate in terms of reproducibility. Therefore, five different layup configurations, as shown in Table 7, are investigated. These differ in the number of steel and CFRP plies and their position in the laminate stack. The different layup variations result in specimen thicknesses between around 0.5 mm and 1 mm. Furthermore, the metal volume fraction (MVF) varies between 12 % and 24 %.

From Figure 10 it can be seen that with increasing specimen thickness, except for layup ID1412, the radius of the respective specimens increases. Specimens with layup ID13 produced very small radii resulting in difficulties during measurement with the laser scanning technique. Further, the handling of these specimens is more complicated because of their small thickness and hence low stiffness. Therefore, the curvature measurements can be influenced by gravitation, which depends on the placement of the specimen during the measurement. On the other hand, the specimens with ID1412 are not covered by the analytical solution anymore since they do not represent a classic bimetal. Therefore, these two laminates (ID13 and ID1412) are excluded from any further considerations in the context of this work. Likewise, the layup ID15 is excluded to have a greater difference in terms of thickness and MVF between the two remaining layups. Nevertheless, all layups

Preprints (www.preprints.org) | NOT PEER-REVIEWED | Posted: 19 September 2022 doi:10.20944/preprints202209.0251.v1

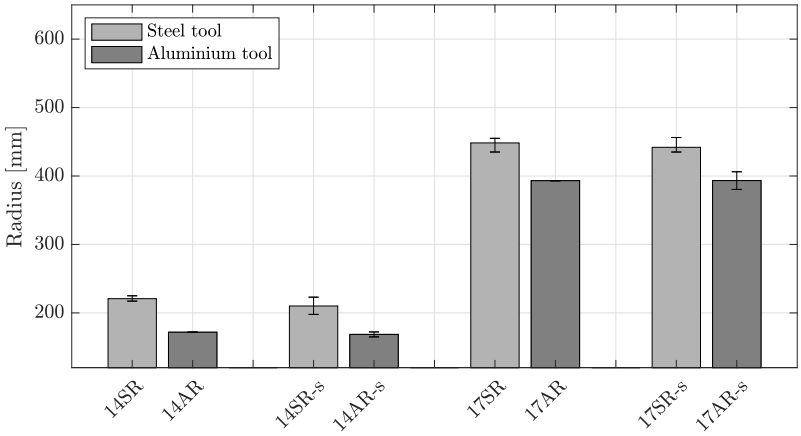

Figure 11. Specimens manufactured on the aluminum tool show significantly smaller radii compared to the specimen manufactured on the steel tool

showed comparable standard deviations during curvature measurements. However, it will be shown in a subsequent section that larger radii show better agreement with the analytical and numerical solution.

The layups with ID14 and ID17 are consequently selected for all the subsequent investigations to determine the influence of the different variables during manufacturing on the curvature.

3.1.2. Influence of tool material on specimen curvature

One great extrinsic contributor to the residual stress level in an FML is the material of the tool [45]. Therefore, two common tool materials in composite manufacturing, steel and aluminum, are chosen to compare their influence on the specimen curvature. The results are shown in Figure 11 for the two selected layups (ID14 and ID17).

It is obvious that specimens manufactured on the aluminum tool show a smaller radius for all investigated configurations compared to the specimens manufactured on the steel tool. This effect can be attributed to the mismatch of the coefficients of thermal expansion between laminate and tool, which results in warpage of the specimen after manufacturing. The steel tool and cover plates show a similar thermal expansion behavior as the steel plies in the laminate themselves (approx. 19 ppm/K, cf. Table 4). The aluminum tool and cover plates, however, possess higher coefficients of thermal expansion of around 24 ppm/K. Hence, using the aluminum tool, the layers close to the tool surface are pre-strained during the heating phase before curing since the aluminum experiences higher thermal expansion. This results in a strain gradient through the thickness of the specimen. These strains are superpositioned with the thermal cure strains resulting from the thermal incompatibility between steel and CFRP layers and are locked into the laminate during resin solidification. After demolding, this results in a different curvature compared to the specimens manufactured on the steel tool. Although the specimens were separated from the tool by using release film, the autoclave pressure and vacuum increase the friction coefficient between the laminate and tool. Since the steel tool and metal layer in the laminate have comparable CTEs, the effect of warpage is not as relevant for the specimens manufactured on the steel tool.

3.1.3. Influence of cure cycle on specimen curvature

The other important extrinsic parameter affecting the residual stress state in a laminate is the cure cycle and in particular the temperature profile during cure. Therefore, two different cure cycles that were developed for residual stress manipulation are taken from the literature and compared to each other in terms of specimen curvature (cf. Section 2.5.1). To assure a significant comparison, specimens with layup ID14 and ID17 are manufactured during two production runs, while at the same time the two tool materials and three

Preprints (www.preprints.org) | NOT PEER-REVIEWED | Posted: 19 September 2022 doi:10.20944/preprints202209.0251.v1

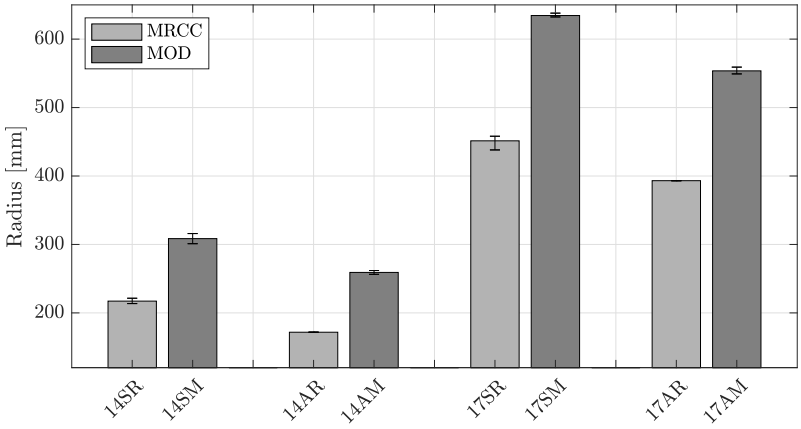

Figure 12. The modified cure cycle (MOD) clearly increases the radius of asymmetric specimens compared to the manufacturer-recommended cure cycle (MRCC), independent of tool material and specimen layup

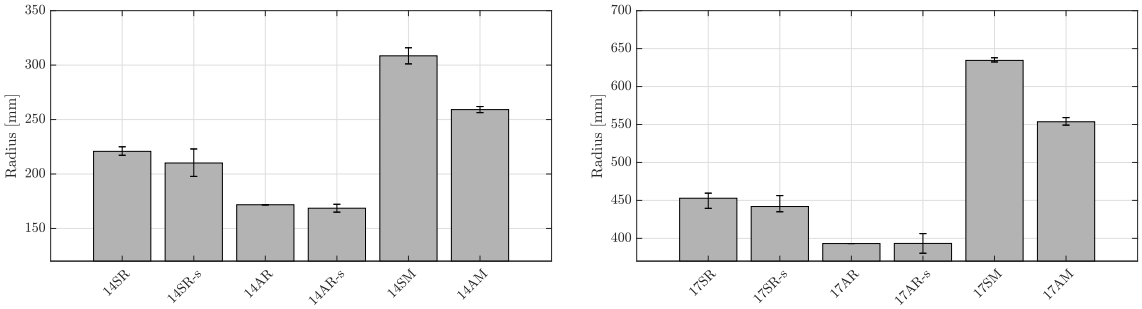

(a) Specimens with layup ID14 **(b)** Specimens with layup ID17

Figure 13. Difference in specimen radius due to variations in the cure cycle, tool material, and manufacturing setup

manufacturing setups are used. This is achieved by using two different tools within the same autoclave loading. The resulting curvatures for the specimens manufactured in these two cure cycles are shown in Figure 12.

The plot shows, that the two different cure cycles can be clearly distinguished by the radius of the specimens. For all specimens, the MOD cure cycle shows larger radii compared to the MRCC. This behavior is expected since the MOD cycle was developed to reduce residual stresses in a specimen, which consequently results in less curvature and hence larger radii. The MOD cure cycle increases the radius by 42 to 50 % for the specimens with ID14 and by around 40 % for the specimens with ID17.

3.1.4. Comparison of curvatures across all specimens

In Figure 13 the radii of all specimens are plotted for the layups ID14 (Figure 13a) and ID17 (Figure 13b) for general comparison. The two main influencing factors, tool material and cure cycle, clearly distinguish the different curvature levels, which is particularly pronounced in layup ID17.

Furthermore, slight deviations can be recognized within the specimens with identical cure cycle and tool material, but different manufacturing setups. The stacked setup, indicated by "-s" in the specimen ID, tendentially shows smaller radii and a larger standard deviation compared to the specimens manufactured on their own between tool and cover plate.

During visual inspection of the specimens manufactured with the stacked setup, revealed that the CFRP face of these specimens shows a high surface roughness. Whereas the specimens manufactured solely between tool and cover plate possess a surface roughness comparable to the surface of the tool. The high roughness of the stacked specimens can

Preprints (www.preprints.org) | NOT PEER-REVIEWED | Posted: 19 September 2022 doi:10.20944/preprints202209.0251.v1

be explained by the lack of a rigid metal tool or cover plate on the CFRP surface. This leads to the fibers interacting with the surface of the opposite specimen since they are only separated by a thin release film. As a result, the surface roughness leads to locally varying laminate thicknesses and hence local differences in bending stiffness and metal volume fractions. These differences increase the variability in the curvature evaluation and complicate the comparability to analytical and numerical derived values. Therefore, the stacked manufacturing setup with CFRP facing CFRP is not recommended by the authors for further investigations.

3.2. Correlation of curvature and stress-free temperature

Not only the curvature but also the stress-free temperature for all the specimens was determined in a laboratory oven using the method described in Section 2.1.2. In Figure 14, the resulting stress-free temperatures for all specimens of the layups ID14 and ID17 are plotted against their radii. The two different layup configurations can be clearly distinguished by the radius. However, the stress-free temperatures are rather independent of the layup and only sensitive to the extrinsic parameters like tool material (A: aluminum and S: steel) and cure cycle (R: MRCC and M: MOD). The different extrinsic influences can be differentiated independently of the layup through the horizontal lines in the figure. For the layup with ID14, there is slightly more scattering within the experimental data, which could already be seen in Figure 13a compared to the layup with ID17 (Figure 13b).

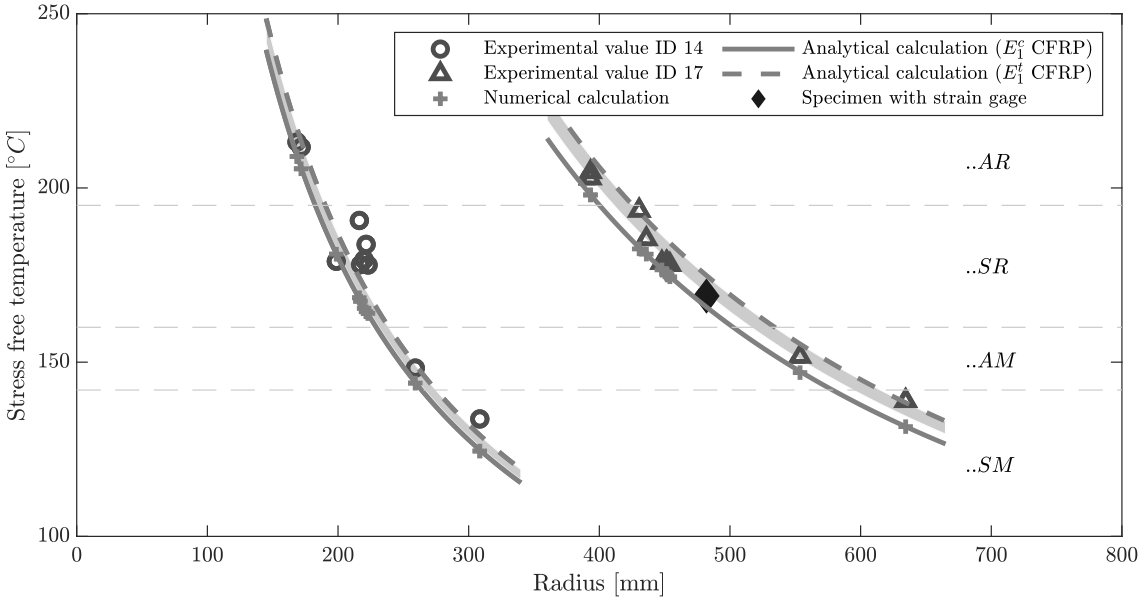

Figure 14. Correlation of stress-free temperature with specimen radius and comparison to analytical and numerical derived values. Specimens are clustered according to their stress-free temperature and the two extrinsic influencing factors tool material and cure cycle

Furthermore, the analytical correlation (see Equation 1) between the radius and stress-free temperature is calculated for the respective layups and added to the figure. The dashed lines represent this solution calculated with the material parameters given in Table 4. The analytics provide a good fit for the experimental data.

From the 3D-optical measurements of every specimen, it is found that the specimen thickness in reality is slightly smaller than the nominal thickness. This can also be observed in Figure 1b, where the mean specimen thickness shows to be approximately 0.625-0.63 mm compared to the nominal thickness of 0.64 mm for that specimen. Therefore, the grey area around the analytical solution in Figure 14 shows the uncertainty due to a reduction in specimen thickness by 0.015 mm assuming a constant thickness ratio m in Equation 1.

Preprints (www.preprints.org) | NOT PEER-REVIEWED | Posted: 19 September 2022 doi:10.20944/preprints202209.0251.v1

Table 8. Uncertainties in material parameters and their consequence for the analytical stress-free temperature calculation from given radius

FML constituent	Material parameter	Variation	Direction of change in T_{sf}
CFRP	t	↑	↑
	E	↑	↑
	α	↑	↑
Steel	t	↑	↓
	E	↑	↓
	α	↑	↓

Changing the thickness ratio m has an even larger effect on the analytical solution because the thickness ratio m enters the equation with a higher power. Reducing the steel ply thickness increases the respective stress-free temperature, while a reduction of the CFRP ply thickness reduces the stress-free temperature for a given radius. From Equation 1 it can be seen that the ply thickness is the most sensitive parameter in the analytical solution. However, uncertainties in the other material parameters, i.e. stiffness and coefficient of thermal expansion, can also influence the analytical results. Table 8 shows the direction of the influence on T_{sf} when increasing each parameter for a given radius.

Remembering the stress state from Figure 5, it is clear that the CFRP layers are in a compressive stress state. Therefore, the question arises whether the tensile modulus is the relevant material parameter. Table 8 reveals that reducing the modulus of elasticity to its compressive value given in Table 4, results in reduced stress-free temperatures. This is also shown in Figure 14 for the analytical solution with E_1^c as calculation parameter. The result is lower stress-free temperatures for a given radius. From the Figure and the correlation of the data points, however, it cannot be concluded whether the compression modulus E_1^c increases the agreement between experiment and analytic solution.

The numerical results derived from the FEA model, as described in Section 2.3, are congruent to the analytical solutions. In Figure 14 the numerical calculated stress-free temperatures are plotted exemplary for the the analytical solution using E_1^c and the relevant discrete radii.

3.3. Transformation into residual stresses and validation using the strain gage method

In the previous chapter, it was shown, that the correlation between curvature and stress-free temperature within the experimental data is also found in the analytical and numerical solutions. Furthermore, it could be proven, that the stress-free temperature is rather independent of the layup. Therefore, it can be assumed that laminates manufactured within the same process cycle on the same tool possess the same stress-free temperature T_{sf}. This T_{sf} can consequently be used to calculate the resulting residual stresses for all the laminates within the same batch, using Equation 2.

To validate this, the strain gage technique described in Section 2.1.3 is used. A specimen with layup ID17 is equipped with a strain gage on the metal ply (cf. Figure 3) and consequently cured in the autoclave on a steel tool using the MRCC. The resulting curvature and stress-free temperature likewise is plotted into Figure 14. Again it correlates very well with the analytical solution. However, it slightly deviates from the other specimens manufactured with the same tool and cure cycle. This can potentially be attributed to the different manufacturing runs, the strain gage bonded to the specimen, and the fact that no trimming was used for this specimen to not damage the strain gage.

The resulting strain measurements over temperature, recorded with the strain gage throughout the entire manufacturing cycle are shown in Figure 15a. The progression of the strain curve is consistent with previous strain measurements (cf. [8]). However, at the final cure temperature of 180 °C, the strain gage signal was lost but could be recovered after cooling down to room temperature. Therefore, the strains during cool-down result from linear interpolation between the last recorded value at 180 °C and the first recorded

Preprints (www.preprints.org) | NOT PEER-REVIEWED | Posted: 19 September 2022 doi:10.20944/preprints202209.0251.v1

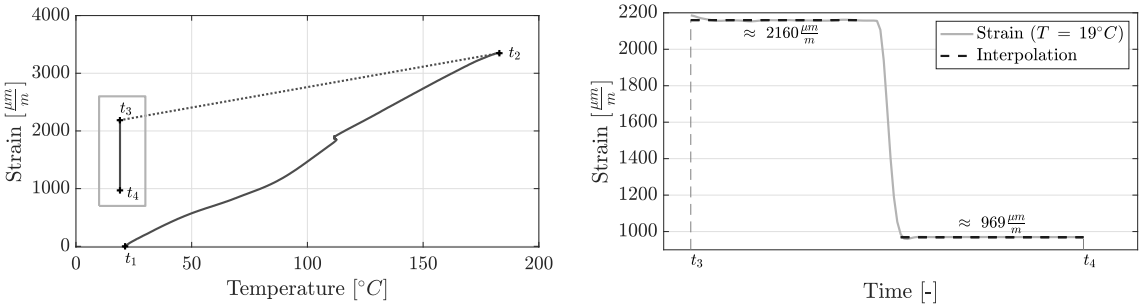

(a) Strains over temperature during cure

(b) Strains over time during demolding

Figure 15. Strain gage recordings during manufacturing and demolding of the instrumented asymmetric specimen. Strain readings start at t_1 and finish at t_4

Table 9. Comparison of measured strains (strain gage) and calculated strains using measured curvature or measured T_{sf}. Values are given for compression and tension moduli of the CFRP material at a reference temperature of $T_r = 21\,°C$. The strain delta indicates the difference between measured and calculated strains. Right hand arrows indicate calculated values with the input parameters to their left

		Radius (mm)	T_{sf} (°C)	Strain flat ($\mu m\,m^{-1}$)	Strain delta (%)
	Experiment	GOM ATOS: 482	Oven: 169	Strain gage: 2175	-
E_1^t	Strain from exp. T_{sf}	-	169	$\rightarrow$ 2320	+6.7
E_1^t	Strain from exp. radius	482	$\rightarrow$176	$\rightarrow$ 2429	+11.7
E_1^c	Strain from exp. T_{sf}	-	169	$\rightarrow$ 2270	+4.4
E_1^c	Strain from exp. radius	482	$\rightarrow$166	$\rightarrow$ 2224	+2.3

value at room temperature which is indicated by the dotted line. The strains during cool down ($t_2 \rightarrow t_3$) are expected to be rather linear as was shown in [8]. Therefore, no error is assumed to be introduced due to the malfunction of the strain gage. During demolding of the specimen from the tool surface at room temperature after curing ($t_3 \rightarrow t_4$), a significant decrease in the residual strain level can be observed. The specimen transitions from its flat state on the tool into the curved state, while releasing some of the inherent residual strains through geometric distortion.

Figure 15b zooms into the demolding step and shows the strains over time. When the specimen is still in its flat state, because the vacuum bag is forcing the specimen onto the flat tool surface, a strain level of 2160 $\mu m\,m^{-1}$ is measured in the metal ply. After demolding, the asymmetric specimen is allowed to relieve some of the introduced stresses through deformation. Consequently, the measured residual strain in the metal ply rapidly reduces to 696 $\mu m\,m^{-1}$.

The experimentally determined parameters of the instrumented specimen can now be compared to different calculation strategies. Table 9 shows the experimental values for a reference temperature of 21 °C. The deviations between the values in Figure 15b and Table 9 result from the different temperature levels. While the strain gage measurements were taken at 19 °C, the values in the table were interpolated for a room temperature of 21 °C since the curvature measurements were taken in a controlled lab environment at a temperature of 21 °C.

At the bottom of Table 9 the resulting strains are calculated by using the measured stress-free temperature and by using the measured radius of the specimen, respectively. The results show, that using the experimentally determined T_{sf}, yields slightly higher calculated residual strains (+145 $\mu m\,m^{-1}$). If the measured radius is taken as a starting point and a

 doi:10.20944/preprints202209.0251.v1

corresponding stress-free temperature is determined with the aid of the analytical solution, the result is a residual strain that is +254 µm m^{-1} higher than in the SG measurement.

This calculation is less sensitive to a change in thickness of the individual layers, as was the case during the analytical curvature determination. However, using the reduced modulus of elasticity due to the fact that compressive stresses act within the CFRP plies, results in strains that are closer to the experimentally determined strain in the flat state. By using E_1^c for the CFRP, the deviations between CLT and experiment can be reduced to values below 5 %.

The results of the combined experiment show, that both approaches either using the stress-free temperature or the specimens curvature are likewise applicable to determine the residual strains in an FML. With this in mind, the relevant stress-free temperatures can likewise be used to calculate the residual strains or stresses in an arbitrary laminate manufactured with the same process parameters using Equation 2.

4. Discussion

An essential finding of this work is the fact that the stress-free temperature is independent of the layup and only sensitive to extrinsic process parameters. Hence, information derived from asymmetric specimens can be directly used to quantify the residual stress state in laminates with different and more complex layups. Therefore, the use of asymmetric specimens seems to be a suitable method to monitor manufacturing processes and determine residual stress states in FML.

However, the influence of warpage needs to be considered to avoid false assumptions. While warpage mainly affects laminates with thicknesses below 1 mm, thick laminates are not affected [25]. The asymmetric laminates in this work are all in the range of 0.5-1 mm and the tool material shows to be a significant contributor to the residual stress state in the specimens. However, for a thicker laminate, this does not necessarily need to hold true. Therefore, it is assumed that by keeping the influence of the tool within the asymmetric specimens to a minimum by using compliant tool CTEs, the accuracy of the proposed method is increased.

The use of asymmetric samples for process monitoring and in particular for residual stress quantification is shown schematically in the form of a flow chart in Figure 16. The boxes framed with thick lines in the Figure indicate the focus of this work.

It was shown, that the curvature and stress-free temperature of asymmetric laminates can be accurately determined using experimental methods. However, curvature measurement using a 3-dimensional scanning head seems to be the most accurate method compared to the T_{sf}-determination or other curvature measurement techniques and is, therefore, to be preferred. During curvature measurements, it is important to also determine the ambient temperature because it is needed as a reference temperature during subsequent calculations.

Furthermore, the results reveal that a significant correlation between curvature and stress-free temperature exists for asymmetric specimens. However, the laminate layup, the manufacturing setup, and the specimen post-processing need to be considered to reduce the scattering within the experimental data. Thicker laminates that result in larger radii are favorable. Thin laminates and consequently small radii could potentially introduce non-linear effects, that increase scattering and can lead to deviations between experiment and analytical solution. Furthermore, the manufacturing setup where two specimens are placed on top of each other with their CFRP sides is to be avoided. It is assumed that a setup where the steel sides face each other shows comparable results to the single setups. However, this placement strategy was not investigated in this work. A trimming operation after curing of the specimens is recommended to reduce the influence of edge effects on the evaluated parameter. It is assumed that trimming reduces the scattering within the experimental results, however, the difference was not quantified within this work. It is recommended to use water-jet cutting instead of a saw to reduce any thermal influences on the specimen state.

Preprints (www.preprints.org) | NOT PEER-REVIEWED | Posted: 19 September 2022 doi:10.20944/preprints202209.0251.v1

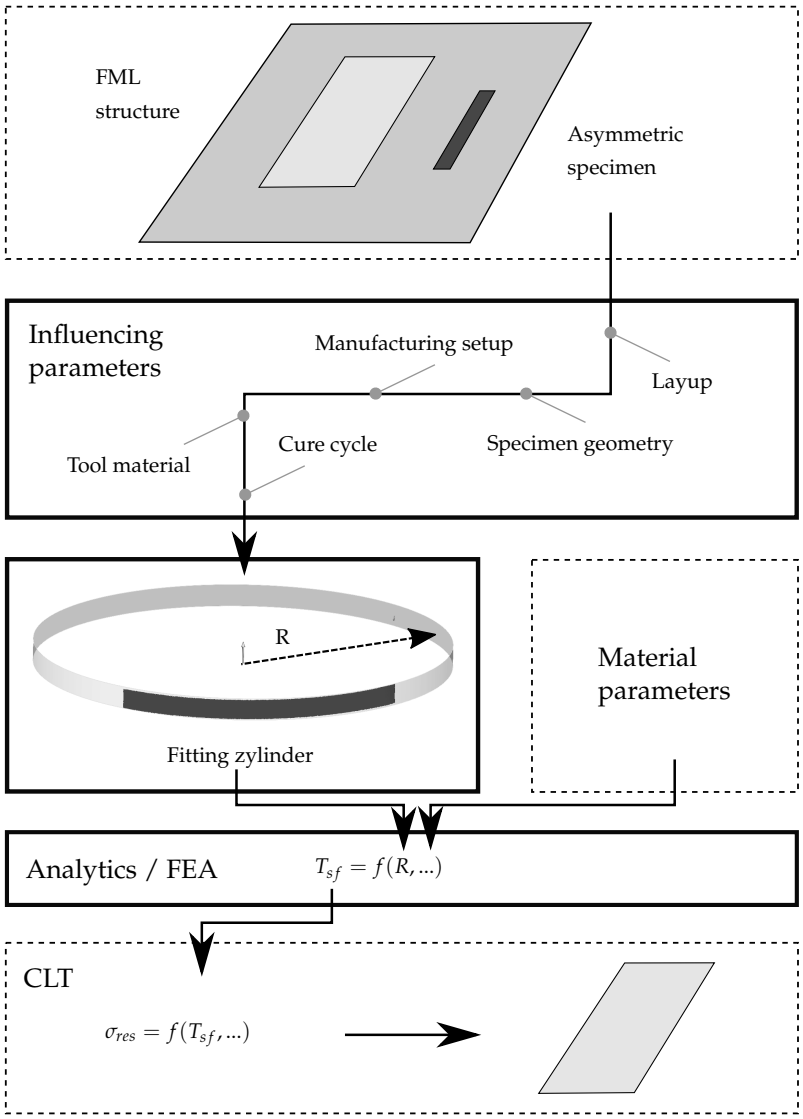

Figure 16. Proposed workflow to use asymmetric specimens for residual stress quantification of FML structures. The focus of this paper is indicated by the boxes framed with thick lines

Analytical and numerical methods are likewise able to depict the correlation between curvature and T_{sf}. However, it was shown that both solutions are very sensitive to uncertainties in the specimen thickness and material parameters. Therefore, a comprehensive set of material parameters is necessary for accurate calculations. To have more accurate thickness information, an analysis of a cross-sectional cut could be integrated into the process. Moreover, in this work, only the modulus of elasticity of the steel material was experimentally determined. All other material parameters were taken from the literature. To improve the results in future research, the other relevant material parameters should also be verified by experiments.

The parameters derived from the asymmetric specimen are in accordance with in-situ strain gage measurements. Depending on the material parameters used, deviations below 5 % and 12 % could be achieved. In the next step, this validation needs to be verified for a larger specimen set and different parameter variations as well as for a more complex FML structure. This is indicated by the top and bottom boxes in Figure 16. Besides the classical laminate theory, this step can also be coupled with an FEA model such that the stress-free temperature is used as an input parameter within this model. This way, also more complex stress states due to complex layups and geometries could be described.

5. Conclusion

In this work, it was shown that the accuracy of the curvature analysis of asymmetric specimen to determine the residual stress state in an FML highly depends on appropriate laminate layups, evaluation techniques and comprehensive material parameters. Thin laminates are assumed to show non-linear effects and are further prone to additional influences due to warpage. Therefore, thicker asymmetric laminates that result in larger radii are to be preferred in combination with CTE compliant tools. Furthermore, by using a small width-to-length aspect ratio, effects due to transverse curvatures can be neglected.

When considering the influencing parameters carefully, a good correlation between the curvature and stress-free temperature of asymmetric specimens can be achieved, that is in accordance with analytical and numerical solutions. Hence, the stress-free temperature gained from such asymmetric laminates can consequently be used for the residual stress quantification in more complex FML structures manufactured within the same process. The proposed workflow in Figure 16 highlights the steps to be followed. Future work needs to mainly concentrate on the validation of the transfer of residual stress levels from asymmetric specimens to a complex structure.

The findings in this work are not only valid for FMLs but it is assumed that they can also be adapted to other lamianted composite materials. However, due to the high anisotropy of the FML, the effects considered are more prominent in an FML consisting of CFRP and steel.

Author Contributions: Conceptualization, Johannes Wiedemann, Jan-Uwe Schmidt and Christian Hühne; Data curation, Johannes Wiedemann and Jan-Uwe Schmidt; Formal analysis, Johannes Wiedemann and Jan-Uwe Schmidt; Funding acquisition, Christian Hühne; Investigation, Johannes Wiedemann and Jan-Uwe Schmidt; Methodology, Johannes Wiedemann and Jan-Uwe Schmidt; Project administration, Christian Hühne; Supervision, Christian Hühne; Validation, Johannes Wiedemann and Jan-Uwe Schmidt; Visualization, Johannes Wiedemann and Jan-Uwe Schmidt; Writing – original draft, Johannes Wiedemann and Jan-Uwe Schmidt; Writing – review & editing, Johannes Wiedemann, Jan-Uwe Schmidt and Christian Hühne.

Funding: The authors expressly acknowledge the financial support for the research work on this article within the Research Unit 3022 "Ultrasonic Monitoring of Fibre Metal Laminates Using Integrated Sensors" by the German Research Foundation (Deutsche Forschungsgemeinschaft (DFG)).

Data Availability Statement: The data presented in this study are available on request from the corresponding author. The data are not publicly available due to ongoing studies.

Acknowledgments: The authors acknowledge support by the Open Access Publication Funds of Technische Universität Braunschweig.

Conflicts of Interest: The authors declare no conflict of interest. The funders had no role in the design of the study; in the collection, analyses, or interpretation of data; in the writing of the manuscript, or in the decision to publish the results.

References

1. Alderliesten, R. *Fatigue and fracture of fibre metal laminates*; Vol. 236, *Solid mechanics and its applications*, Springer: Cham, 2017.
2. Vlot, A.; Gunnink, J.W. *Fibre Metal Laminates: An Introduction*; Springer Netherlands: Dordrecht, 2001.
3. Petersen, E.; Stefaniak, D.; Hühne, C. Experimental investigation of load carrying mechanisms and failure phenomena in the transition zone of locally metal reinforced joining areas. *Composite Structures* **2017**, *182*, 79–90. doi:10.1016/j.compstruct.2017.09.002.
4. Boose, Y.; Kappel, E.; Stefaniak, D.; Prussak, R.; Pototzky, A.; Weiß, L. Phenomenological investigation on crash characteristics of thin layered CFRP-steel laminates. *International Journal of Crashworthiness* **2020**, *182*, 1–10. doi:10.1080/13588265.2020.1787681.
5. Düring, D.; Petersen, E.; Stefaniak, D.; Hühne, C. Damage resistance and low-velocity impact behaviour of hybrid composite laminates with multiple thin steel and elastomer layers. *Composite Structures* **2020**, *238*, 111851. doi:10.1016/j.compstruct.2019.111851.
6. Abouhamzeh, M. Distortions and Residual Stresses of GLARE Induced by Manufacturing. PhD thesis, Delft University of Technology, 2016. doi:10.4233/uuid:1f1b3e5c-72b8-440c-8d98-4b4c82814fb6.
7. Kappel, E.; Prussak, R.; Wiedemann, J. On a simultaneous use of fiber-Bragg-gratings and strain-gages to determine the stress-free temperature Tsf during GLARE manufacturing. *Composite Structures* **2019**, *227*. doi:10.1016/j.compstruct.2019.111279.
8. Wiedemann, J.; Prussak, R.; Kappel, E.; Hühne, C. In-situ quantification of manufacturing-induced strains in fiber metal laminates with strain gages. *Composite Structures* **2022**, *Vol. 691*, 115967. doi:10.1016/j.compstruct.2022.115967.

9. Zobeiry, N.; Poursartip, A. The origins of residual stress and its evaluation in composite materials. In *Structural integrity and durability of advanced composites*; Beaumont, P.W.R., Ed.; Woodhead publishing series in composites science and engineering, Elsevier: Amsterdam, 2015; pp. 43–72. doi:10.1016/B978-0-08-100137-0.00003-1.
10. Luyckx, G.; Voet, E.; Lammens, N.; Degrieck, J. Strain measurements of composite laminates with embedded fibre bragg gratings: criticism and opportunities for research. *Sensors (Basel, Switzerland)* **2011**, *11*, 384–408. doi:10.3390/s110100384.
11. Tsukada, T.; Takeda, S.; Minakuchi, S.; Iwahori, Y.; Takeda, N. Evaluation of the influence of cooling rate on residual strain development in unidirectional carbon fibre/polyphenylenesulfide laminates using embedded fibre Bragg grating sensors. *Journal of Composite Materials* **2017**, *51*, 1849–1859. doi:10.1177/0021998316662327.
12. Prussak, R.; Stefaniak, D.; Hühne, C.; Sinapius, M. Evaluation of residual stress development in FRP-metal hybrids using fiber Bragg grating sensors. *Production Engineering* **2018**, *12*, 259–267. doi:10.1007/s11740-018-0793-4.
13. Twigg, G.; Poursartip, A.; Fernlund, G. An experimental method for quantifying tool–part shear interaction during composites processing. *Composites Science and Technology* **2003**, *63*, 1985–2002. doi:10.1016/S0266-3538(03)00172-6.
14. Crasto, A.S.; Kim, R.Y. On the Determination of Residual Stresses in Fiber-Reinforced Thermoset Composites. *Journal of Reinforced Plastics and Composites* **1993**, *12*, 545–558. doi:10.1177/073168449301200505.
15. Unger, W.J.; Hansen, J.S. The Effect of Cooling Rate and Annealing on Residual Stress Development in Graphite Fibre Reinforced PEEK Laminates. *Journal of Composite Materials* **1993**, *27*, 108–137. doi:10.1177/002199839302700201.
16. Cowley, K.D.; Beaumont, P.W. The measurement and prediction of residual stresses in carbon-fibre/polymer composites. *Composites Science and Technology* **1997**, *57*, 1445–1455. doi:10.1016/S0266-3538(97)00048-1.
17. Prussak, R.; Stefaniak, D.; Hühne, C.; Sinapius, M. Residual Stresses in Intrinsic UD-CFRP-Steel-Laminates - Experimental Determination, Identification of Sources, Effects and Modification Approaches. 20th Symposium on Composites. Trans Tech Pubn, 2015, Materials Science Forum, pp. 369–376. doi:10.4028/www.scientific.net/MSF.825-826.369.
18. Jeronimidis, G.; Parkyn, A.T. Residual Stresses in Carbon Fibre-Thermoplastic Matrix Laminates. *Journal of Composite Materials* **1988**, *22*, 401–415. doi:10.1177/002199838802200502.
19. Schulte, K.J.; Hahn, H.T. Prediction and Control of Processing-Induced Residual Stresses in Composites. Part 2: AS4/PEEK Composite, Pennsylvania State University Composites Manufacturing Technology Center: Final Technical Report.
20. O'Brien, T.K. Fatigue Delamination Behavior of PEEK Thermoplastic Composite Laminates. *Journal of Reinforced Plastics and Composites* **1988**, *7*, 341–359. doi:10.1177/073168448800700403.
21. Pagano, N.J.; Hahn, H.T. Evaluation of Composite Curing Stresses. In *Mechanics of Composite Materials*; Gladwell, G.M.L.; Reddy, J.N., Eds.; Springer Netherlands: Dordrecht, 1994; Vol. 34, *Solid mechanics and its applications*, pp. 57–69.
22. Prussak, R.; Stefaniak, D.; Kappel, E.; Hühne, C.; Sinapius, M. Smart cure cycles for fiber metal laminates using embedded fiber Bragg grating sensors. *Composite Structures* **2019**, *213*, 252–260. doi:10.1016/j.compstruct.2019.01.079.
23. Schürmann, H. *Konstruieren mit Faser-Kunststoff-Verbunden*; Springer Berlin Heidelberg: Berlin, Heidelberg, 2007. doi:10.1007/978-3-540-72190-1.
24. Both, J.C. *Tragfähigkeit von CFK-Metall-Laminaten unter mechanischer und thermischer Belastung: Zugl.: München, Techn. Univ., Diss., 2014*; Ingenieurwissenschaften, Dr. Hut: München, 2014.
25. Albert, C.; Fernlund, G. Spring-in and warpage of angled composite laminates. *Composites Science and Technology* **2002**, *62*, 1895–1912. doi:10.1016/S0266-3538(02)00105-7.
26. Kappel, E.; Stefaniak, D.; Fernlund, G. Predicting process-induced distortions in composite manufacturing – A pheno-numerical simulation strategy. *Composite Structures* **2015**, *120*, 98–106. doi:10.1016/j.compstruct.2014.09.069.
27. Potter, K.D.; Campbell, M.; Langer, C.; Wisnom, M.R. The generation of geometrical deformations due to tool/part interaction in the manufacture of composite components. *Composites Part A: Applied Science and Manufacturing* **2005**, *36*, 301–308. doi:10.1016/j.compositesa.2004.06.002.
28. Stefaniak, D.; Kappel, E.; Spröwitz, T.; Hühne, C. Experimental identification of process parameters inducing warpage of autoclave-processed CFRP parts. *Composites Part A: Applied Science and Manufacturing* **2012**, *43*, 1081–1091. doi:10.1016/j.compositesa.2012.02.013.
29. White, S.R.; Hahn, H.T. Cure Cycle Optimization for the Reduction of Processing-Induced Residual Stresses in Composite Materials. *Journal of Composite Materials* **1993**, *27*, 1352–1378. doi:10.1177/002199839302701402.
30. Kim, H.S.; Park, S.W.; Lee, D.G. Smart cure cycle with cooling and reheating for co-cure bonded steel/carbon epoxy composite hybrid structures for reducing thermal residual stress. *Composites Part A: Applied Science and Manufacturing* **2006**, *37*, 1708–1721. doi:10.1016/j.compositesa.2005.09.015.
31. Kim, Y.K.; Daniel, I.M. Cure Cycle Effect on Composite Structures Manufactured by Resin Transfer Molding. *Journal of Composite Materials* **2002**, *36*, 1725–1743. doi:10.1177/0021998302036014598.
32. Kim, S.S.; Murayama, H.; Kageyama, K.; Uzawa, K.; Kanai, M. Study on the curing process for carbon/epoxy composites to reduce thermal residual stress. *Composites Part A: Applied Science and Manufacturing* **2012**, *43*, 1197–1202. doi:10.1016/j.compositesa.2012.02.023.
33. Khatkhate, A.M.; Singh, M.P.; Mirchandani, P.T. A Parametric Approximation for the Radius of Curvature of a Bimetallic Strip. *International Journal of Engineering Research and* **2017**, *V6*. doi:10.17577/IJERTV6IS060317.
34. Angel, G.D.; Haritos, G.K. An Immediate Formula for the Radius of Curvature of A Bimetallic Strip. *International journal of engineering research and technology* **2013**, *2*.
35. Timoshenko, S. Analysis of Bi-Metal Thermostats. *Journal of the Optical Society of America* **1925**, *11*, 233. doi:10.1364/JOSA.11.000233.

36. Nettles, A.T. Basic Mechanics of Laminated composite plates: Technical Report: NASA-RP-1351, 1994.
37. Stefaniak, D.; Kappel, E.; Kolesnikov, B.; Hühne, C. Improving the mechanical performance of unidirectional CFRP by metal-hybridization. ECCM15 - 15th European Conference on Composite Materials, 2012.
38. Blohowiak, K.Y.; Osborne, J.H.; Krienke, K.A. Surface pretreatment of metals to activate the surface for sol-gel coating. US5869140A, 1999.
39. Stefaniak, D. Improving residual strength of unidirectionally reinforced plastic laminates by metal layering. Dissertation, Technische Universität Carola-Wilhelmina zu Braunschweig, 2017.
40. 3M Aerospace and Commercial Transportation Division. 3M™ Surface Pre-Treatment AC-130-2, 2015.
41. DIN EN ISO 6892-1:2020-06, Metallische Werkstoffe_- Zugversuch_- Teil_1: Prüfverfahren bei Raumtemperatur (ISO_6892-1:2019); Deutsche Fassung EN_ISO_6892-1:2019. doi:10.31030/3132591.
42. National Institute for Aviation Research - Wichita State University. Hexcel 8552 AS4 Unidirectional Prepreg at 190 gsm & 35% RC Qualification Material Property Data Report, 2011.
43. Hexcel Corporation. Product data sheet HexPly 8552, 2020.
44. Kappel, E. On thermal-expansion properties of more-orthotropic prepreg laminates with and without interleaf layers. *Composites Part C: Open Access* **2020**, *3*, 100059. doi:10.1016/j.jcomc.2020.100059.
45. Wisnom, M.R.; Gigliotti, M.; Ersoy, N.; Campbell, M.; Potter, K.D. Mechanisms generating residual stresses and distortion during manufacture of polymer–matrix composite structures. *Composites Part A: Applied Science and Manufacturing* **2006**, *37*, 522–529. doi:10.1016/j.compositesa.2005.05.019.